analytical chemistry

pubs.acs.org/ac Article

Pyroglutamate Aminopeptidase I Promotes Hepatocellular Carcinoma via IL-6/STAT3 Activation as Revealed by a Specific Biosensor

Wu-Yingzheng Guo,[†] Rong-Rong Li,[†] Yi-Xuan Fu, Shi-Yu Liu, Guo-Zhen Liu, Wen-Chao Yang,* and Guang-Fu Yang

Cite This: *Anal. Chem.* 2021, 93, 13311−13318 Read Online

ACCESS | Metrics & More | Article Recommendations | Supporting Information

ABSTRACT: As a global health challenge, hepatocellular carcinoma (HCC) is strongly associated with chronic inflammation. Targeting inflammation, particularly inflammatory factors, is regarded as an important strategy for HCC diagnosis and treatment. Pyroglutamic aminopeptidase I (PGP-I), a common exopeptidase, was recently identified as a novel inflammatory cytokine in cells. However, whether PGP-I is involved in HCC development and can be regarded as a biomarker remains unclear. To address this issue, endogenous PGP-I was imaged in live cells and *in vivo*, and the related biochemical and pathological processes were analyzed accordingly with a newly developed fluorogenic PGP-I biosensor. Bioimaging with the specific biosensor demonstrated the aberrant expression of PGP-I in HCC cell lines and tumor-bearing nude mice. Moreover, overexpression of PGP-I in HCC cells promoted tumor progression, whereas knockdown of PGP-I significantly suppressed tumor cell growth and migration. The activity of PGP-I was further identified to be highly related to the phosphorylation of STAT3, which could be impeded by the natural product parthenolide. Collectively, these findings suggest that PGP-I, which can promote hepatocellular tumor progression through the classical inflammation-/tumor-related IL-6/STAT3 pathway, may serve as a potential HCC biomarker and therapeutic target.

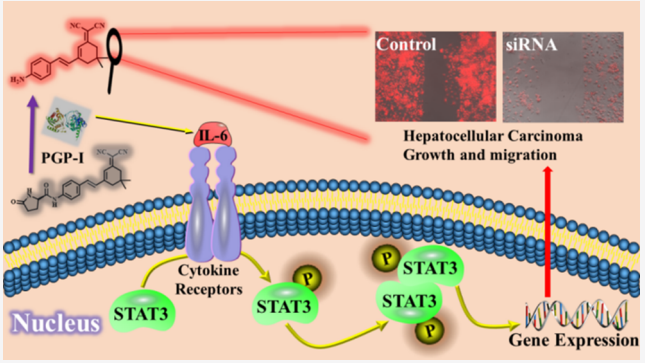

1. INTRODUCTION

Hepatocellular carcinoma (HCC) represents the fifth most common malignancy and the third leading cause of cancer-related death worldwide, with approximately one million new cases diagnosed every year.[1,2] Extensive studies have indicated that HCC is a clear inflammation-related cancer since more than 90% of cases arise in the context of inflammation.[3−5] Hence, targeting inflammation, particularly inflammatory factors, is a key strategy for HCC diagnosis and treatment.[2,6,7] Pyroglutamic aminopeptidase I (PGP-I, EC 3.4.19.3) is a typical cysteine protease that can remove the terminal pyroglutamic acid from proteins or polypeptides, which is of great value in the maintenance of the metabolic equilibrium of proteins and peptides.[8,9] Although the associations of aminopeptidases and various cancers, such as breast cancer, have been reported, the detailed molecular mechanism is very complicated and remains unclear. Recently, with the help of PGP-I-activated fluorescent probes, it was shown that PGP-I was highly linked to the emergence of inflammation in cells and tissues and was regarded as a new inflammatory cytokine.[10−12] The role of PGP-I in the development and progression of cancers such as HCC is still unknown, which may be partially attributed to the unavailability of an efficient biosensor for tracking PGP-I in complex biological systems.

For tracking protease activity, fluorescent probes have attracted increasing attention because of their excellent temporal−spatial resolution, sensitivity, specificity, and ease of operation.[13−20] Inspired by these pioneering works, we intended to explore the detailed relationship between PGP-I and HCC at the molecular level with a desired fluorogenic PGP-I biosensor. Dicyanoisophorone derivative (**DCID**) dyes have a typical push−pull structure and possess a large Stokes shift, excellent membrane permeability, and applicable fluorescence that allows *in vivo* real-time imaging.[21−24] In this study, a fluorogenic biosensor, termed **DCID-pGlu** (Scheme 1) that was developed by another group in a back-to-back study,[12] was applied for reliable monitoring of PGP-I

Received: July 17, 2021
Accepted: September 16, 2021
Published: September 27, 2021

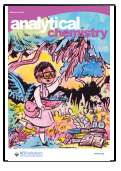

Downloaded via UNIV OF ATHENS on November 4, 2022 at 11:00:25 (UTC).
See https://pubs.acs.org/sharingguidelines for options on how to legitimately share published articles.

ACS Publications © 2021 American Chemical Society

Scheme 1. Schematic Diagram of PGP-I-Involved Mechanism Study with DCID-pGlu

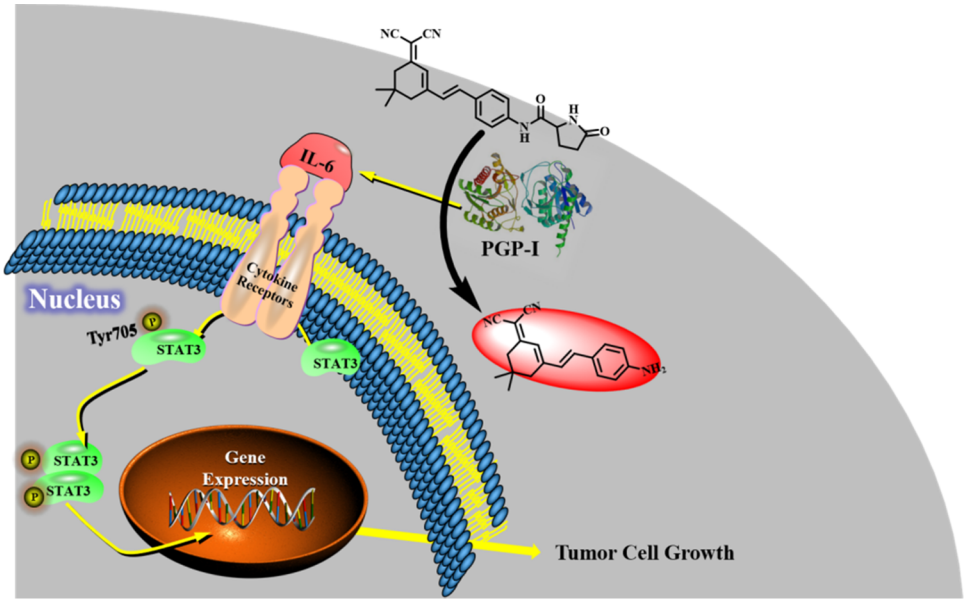

in living cells and *in vivo*. It is worth to mentioning that, although two studies designed the same probe, the major concerns are different. That recent study[12] focused on the validation of the probe to quantify PGP-I in cells and animals, whereas the current study aimed to elucidate the correlation and mechanism of alteration of the PGP-I level with the progression of liver cancer, which has not been reported so far. Using **DCID-pGlu** as a tool, we found that the knockdown of the PGP-I gene caused obvious reductions in the expression levels of proinflammatory cytokine interleukin-6 (IL-6) and phosphorylated signal transducer and activator of transcription 3 (p-STAT3) and thus inhibited the proliferation and migration of liver cancer cells. Moreover, a cellular study suggested that the inhibition of HCC tumor growth by parthenolide may be attributed to the parthenolide-mediated inhibition of PGP-I. These findings demonstrate that PGP-I is a promising biomarker and potential therapeutic target of HCC.

2. EXPERIMENTAL SECTION

2.1. Reagents. The organic solvents and biochemical reagents, such as methylene chloride (DCM), cyclohexanone, phosphorus oxychloride, acetonitrile (ACN), dimethylformamide (DMF), dimethyl sulfoxide (DMSO), 3-(4,5-dimethylthiazol-2-yl)-2,5-diphenyltetrazolium bromide (MTT), iodoacetamide, reduced glutathione (GSH), acetylcholinesterase (AChE), butyrylcholinesterase (BChE), trypsin, chymotrypsin, glutamic-pyruvic transaminase (Glut), carboxypeptidase B (CPB), pig liver esterase (PLE), leucine aminopeptidase (LAP), and Hoest33342, were purchased from Sigma-Aldrich (Shanghai, China). Dipeptidyl peptidase IV (DPP IV), fibroblast activation protein α (FAP-α), and PGP-I were purchased from R&D systems (Minneapolis, MN). Cell culture reagents, such as Roswell Park Memorial Institute-1640 medium (RPMI-1640), Dulbecco's modified Eagle's medium (DMEM), minimum essential medium (MEM), calf serum, and phosphate-buffered saline (PBS), were purchased from Thermo Fisher Scientific (Shanghai, China). Human cell lines, LO2, HepG2, Bel7402, and HuH-7, were purchased from Procell (Wuhan, China). RIPA (radioimmunoprecipitation assay) lysis buffer (CW2333) was purchased from CW Biotech Co. Ltd., (Beijing, China). Agarose, poly(vinylidene fluoride) (PVDF) membranes, anti-TNF-α antibody, gel electrophoresis kits, western blot kits, enhanced chemiluminescence kits (ECL), and BCA protein assay kits were purchased from Beyotime Biotechnology (Shanghai, China). Anti-PGP-1 antibody was purchased from Abcam (Cambridge, MA). The purities of the tested enzymes were judged by Coomassie-stained sodium dodecyl sulphate-polyacrylamide gel electrophoresis (SDS-PAGE). The stock solution (20 mM) of **DCID-pGlu** was prepared by dissolving the requisite amount of it in DMSO. Stock solutions of other substances were prepared by dissolving in PBS or water. Commercial dyes such as MitoTracker Green, LysoTracker Green, and ER-Tracker Green were purchased from Yeasen (Shanghai, China). All other chemicals and biological reagents were of analytical grade or the higher quality commercial grade.

2.2. Instrumentation. UV−vis absorption spectrum and fluorescence spectrum were measured by a microplate reader (Cytation5, BioTek) using a cuvette (Hellma, Germany). The 96-well microplates for the MTT assay were purchased from Sigma-Aldrich (Shanghai, China). High-resolution mass spectra (HRMS) were obtained in positive mode on a MALDI SYNAPT G2 HRMS (ESI; MA). ^{13}C NMR and ^{1}H NMR spectra were scanned in DMSO-d_6 on a Varian Mercury 400 MHz spectrometer, and resonances were given in ppm relative to tetramethylsilane (TMS). The following abbreviations were used to designate chemical shift multiplicities: s, singlet; d, doublet; t, triplet; and m, multiplet.

2.3. PGP-I Assay with DCID-pGlu. The sensing performance of **DCID-pGlu** (10 μM) was evaluated by adding a certain amount of PGP-I in 10 mM PBS at the desired pH and temperature. Using an M5 microplate reader, the fluorescence intensity (FI) of the reaction system was measured at λ_{ex}max = 450 nm and λ_{em}max = 650 nm. The specificity of **DCID-pGlu** for PGP-I was evaluated by calculating the corresponding FI of **DCID-pGlu** (10 μM) against different analytes, including amino acids and commonly used enzymes. All of the data were estimated as averaged values based on three separate measurements.

https://doi.org/10.1021/acs.analchem.1c03011
Anal. Chem. 2021, 93, 13311−13318

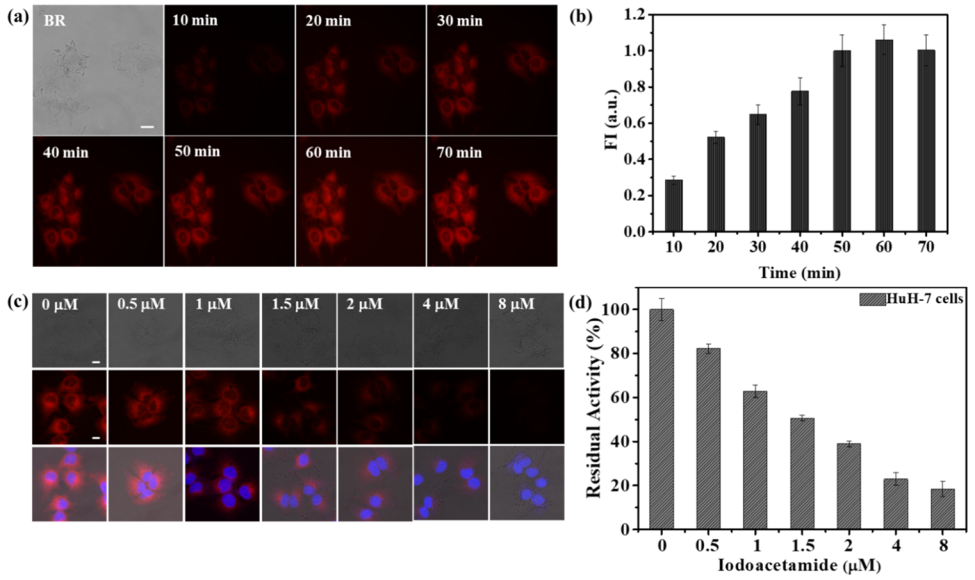

Figure 1. (a) Fluorescence images of HuH-7 cells incubated with **DCID-pGlu** (5 μM) for different times (10, 20, 30, 40, 50, 60, and 70 min). (b) Relative intensities of the corresponding fluorescence images in panel (a) (the pixel intensity from the image at 50 min is defined as 1.0). The results are the mean ± standard deviation of three separate measurements. BR refers to bright field. (c) Fluorescence images of PGP-I in HuH-7 cells. The cells were pretreated with iodoacetamide at various concentrations (0, 0.5, 1.0, 1.5, 2.0, 4.0, and 8.0 μM) for 4 h and then incubated with the 5 μM probe for 50 min. (d) Relative pixel intensities of the images in panel (c) were measured using ImageJ software (the pixel intensity of 0 μM is defined as 1.0). Scale bar: 10 μm.

2.4. Cell Culture and RNA Interference. All of the cells were grown in specially prepared media supplemented with 10% (V/V) heat-inactivated fetal bovine serum (Gibco): MEM for HepG2 cells, complete RPMI-1640 medium for A549 and HCT116 cells, and DMEM for the other three cell lines (HEK 293, SKOV3, and DU145). All of the living cells were cultured at 5% CO_2 and 37 °C. According to the instructions of the manufacturer, cells were transfected with either LipoD293 (SignaGen Laboratories, China) for PGP-I overexpression or a RNAiMAX lipid transfection reagent (Invitrogen) for PGP-I knockdown. We designed small interfering RNAs (siRNAs) and purchased them from Baijiesi Company (Wuhan, China). The sequence of the siRNA is 5′-GTACCAAACAGTCCA-GAGA-3′.

2.5. Live-Cell Imaging. All of the cells were cultivated on 15 mm glass-bottom cell culture dishes with 1.0 mL of culture medium, as described in the previous report.[25] After removing the residual medium from the cells by washing with PBS three times, they were pretreated with inhibitors. Then, the cells were incubated with **DCID-pGlu** (5 μM) for 50 min and Hoechst 33342 (10 μM) for 5 min at 37 °C, followed by fluorescence imaging on a microscope (Olympus IX71, Japan). The imaging data were then analyzed and quantified by ImageJ software (National Institutes of Health, America). Each experiment was repeated three times.

2.6. Live Imaging of *Zebrafish* and Mice. According to our previously reported method,[25] *zebrafish* were raised in E3 embryo media (0.15 mM KCl, 5 mM NaCl, 0.33 mM $CaCl_2$, and 0.33 mM $MgSO_4$; pH = 7.0 ± 1.0) for 3−5 days. Then, they were placed in glass-bottom dishes and pretreated with or without 100 μM tacrine for 4 h before incubation with different concentrations (5, 10, and 20 μM) of **DCID-pGlu** for 4 h. Fluorescence images were obtaibed using the same microscope (Olympus IX71, Japan). HepG2 tumor-bearing mice and normal mice were purchased from Vital River Laboratories (Beijing, China). Fluorescence images were then acquired with a Lago X Spectral Instruments Imaging system (IVIS Lumina, PerkinElmer).

2.7. Western Blotting. Cells were collected and treated with the RIPA buffer, and then the lysates were rotated in a culturing shaking incubator at 4 °C for 30 min and cleared by centrifugation at 10 000*g* at 4 °C for 10 min. After detection of the protein concentration by the BCA kit, lysates of the same protein content were mixed with a loading buffer and denatured at 95 °C for 5 min. Similar amounts of cell lysates and protein ladders were loaded on a 12% SDS/PAGE gel. After electrophoresis, proteins were transferred to a 0.45 μm PVDF transfer membrane and blocked in 1 × TBS-Tween (28360, Thermo Scientific) buffer with 5% BSA. Then, a suitable concentration of the primary anti-PGPEPI-antibody (ab139702, 1:1000) from Abcam, diluted by 1 × TBS-Tween, was incubated with the membrane overnight at 4 °C. After washing the extra primary antibody with TBST, the anti-rabbit horseradish peroxidase-conjugated secondary antibody was added in 1:1000 dilution and incubated for 2 h. At last, ECL kits were used (Millipore, WBKLS0010) and the fluorescence images were obtained by an automatic chemiluminescence analyzer (Tanon-5200, Shanghai, China). Glyceraldehyde-3-phosphate dehydrogenase from Cell Signaling Technology was used at a dilution of 1:10 000 as a reference.

3. RESULTS AND DISCUSSION

3.1. Optical Characterization of DCID-pGlu. The target probe (**DCID-pGlu**) was constructed by conjugating a pGlu moiety as the recognition group with 2-(3-(4-aminostyryl)-5,5-dimethylcyclohex-2-en-1-ylidene) malononitrile (**DCID**) as the fluorophore. The detailed synthesis methods and structural characterizations of **DCID-pGlu** and **DCID** are described in the Experimental Section and Supporting Data (Figures S1−S7). As expected, the pGlu moiety could easily quench the fluorescence of **DCID** and resulted in a low background fluorescence of the entire probe. The entire molecule **DCID-**

https://doi.org/10.1021/acs.analchem.1c03011
Anal. Chem. 2021, 93, 13311−13318

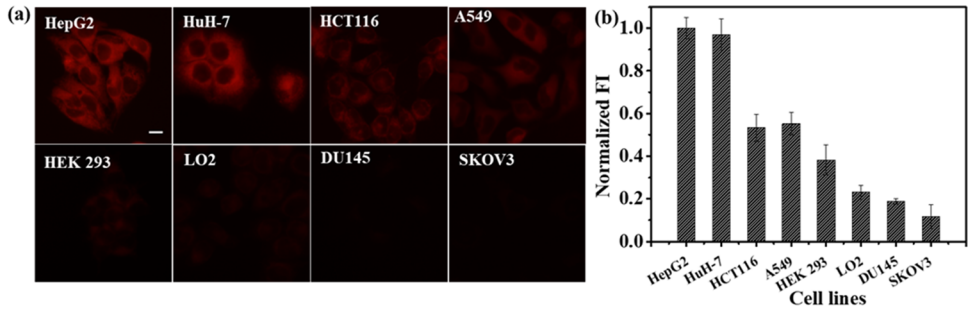

Figure 2. (a) Fluorescence images of different cell lines (DU145, LO2, SKOV3, HCT116, HuH-7, and HepG2). These cells were treated with **DCID-pGlu** (5 μM) for 50 min. (b) Relative pixel intensity of the corresponding fluorescence images in panel (a) (the pixel intensity from the image of HepG2 is normalized as 1.0). Scale bar: 10 μm.

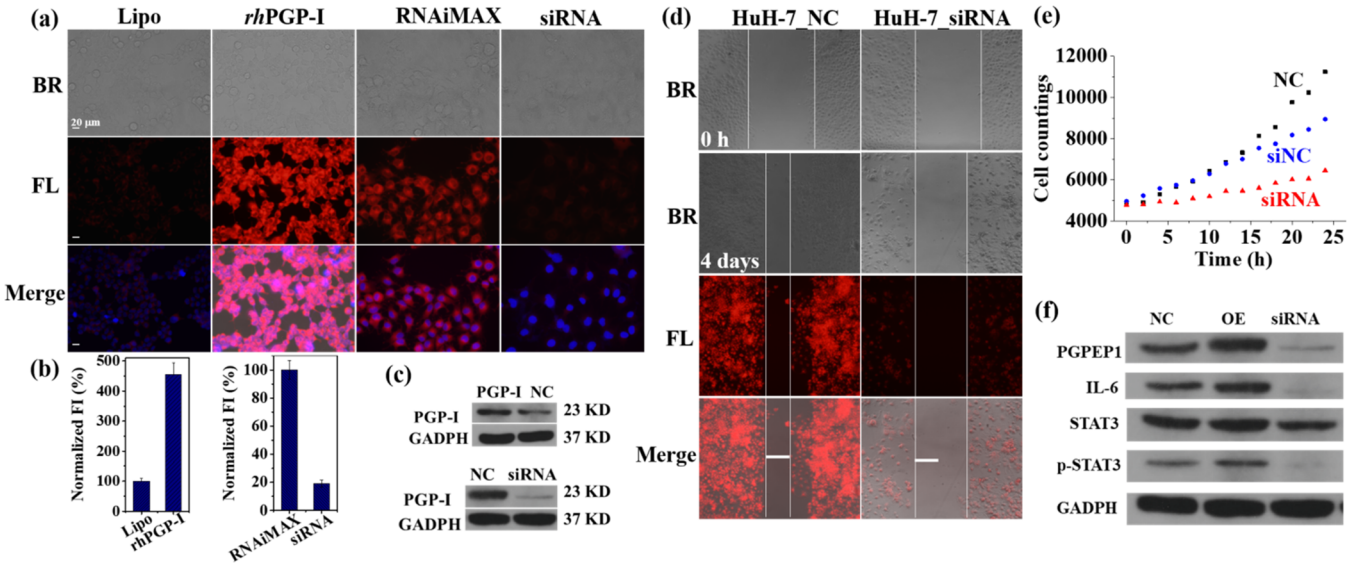

Figure 3. (a) Fluorescence images of *rh*PGP-I-overexpressing HEK 293 cells incubated with **DCID-pGlu** and PGP-I knockdown HuH-7 cells incubated with **DCID-pGlu**. (b) Corresponding fluorescence intensity in cells shown in panel (a). (c) Western blot data of PGP-I expression in *rh* PGP-I-overexpressing HEK 293 cells and PGP-I knockdown HuH-7 cells. (d) Fluorescence imaging analysis of migration in normal HuH-7 cells and cells with PGP-I knockdown via siRNA transfection (cells stained with 5 μM **DCID-pGlu** for 50 min). BR represents bright field and FL represents dark field. Scale bar: 250 μm. (e) Cell proliferation curve of HuH-7 cells under different treatments (NC: cells treated with Lipo; siNC: cells treated with scramble RNA without the transfection reagent; siNC: cells transfected with siRNA). (f) Western blot analysis of PGP-I, STAT3, and p-STAT3 levels in *rh*PGP-I-overexpressing HEK 293 cells and Lipo control (NC: cells treated with Lipo; OE: cells overexpressing *rh*PGP-I).

pGlu exhibited a strong absorption peak at 405 nm and quite weak fluorescence at 550 nm (Figure S8). Upon the addition of PGP-I, the maximum absorption and fluorescence peaks were both red-shifted to 450 and 650 nm, respectively. Thus, the PGP-I-catalyzed reaction could be visualized by the naked eye according to the apparent color change from faint yellow to faint pink and the marked off−on fluorescence enhancement (over 16-fold). The reaction mechanism concerning the liberation of the fluorophore **DCID** from **DCID-pGlu** under the catalysis of PGP-I was verified by high-performance liquid chromatography (HPLC) (Figure S9). The optimization of pH and the working temperature indicated that the FI of **DCID-pGlu** reached the maximum intensity at pH 7.4 and 37 °C when incubated with PGP-I (Figure S10). Under the optimized conditions, the FI of **DCID-pGlu** exhibited a marked enhancement at 650 nm depending on the incubation time and concentration (0−12 ng/mL) of PGP-I (Figure S11). The detection limit for this developed sensor was calculated to be ∼0.31 ng/mL (Figure S12).

Next, the specificity of **DCID-pGlu** against PGP-I was evaluated under the interference of various analytes, including regular amino acids (Asp, GSH, Ser, and Cys) and some representative common hydrolases. The common hydrolases employed here were acetylcholinesterase (AChE), butyrylcholinesterase (BChE), trypsin, chymotrypsin, acid phosphatase (ACP), glutamic-pyruvic transaminase (Glut), carboxylesterase (CE), porcine liver esterase (PLE), and several aminopeptidases, including leucine aminopeptidase (LAP), aminopeptidase N (APN), fibroblast activation protein-α (FAP-α), and dipeptidyl peptidase IV (DPP IV). Intriguingly, only PGP-I triggered dramatic fluorescence enhancement, while none of the other analytes caused significant responses (Figure S11c). As anticipated, the relationship of the reaction velocity versus the **DCID-pGlu** concentration obeyed the Michaelis−Menten equation (Figure S11d). On the basis of the kinetic characterization, **DCID-pGlu** demonstrated a strong binding affinity against PGP-I and could be rapidly hydrolyzed by this enzyme. The results of this kinetic analysis imply that **DCID-pGlu** is a highly specific and sensitive substrate for PGP-I activity assessment.

3.2. Imaging of Endogenous PGP-I in Living Cells. To determine whether **DCID-pGlu** could detect endogenous

https://doi.org/10.1021/acs.analchem.1c03011
Anal. Chem. 2021, 93, 13311−13318

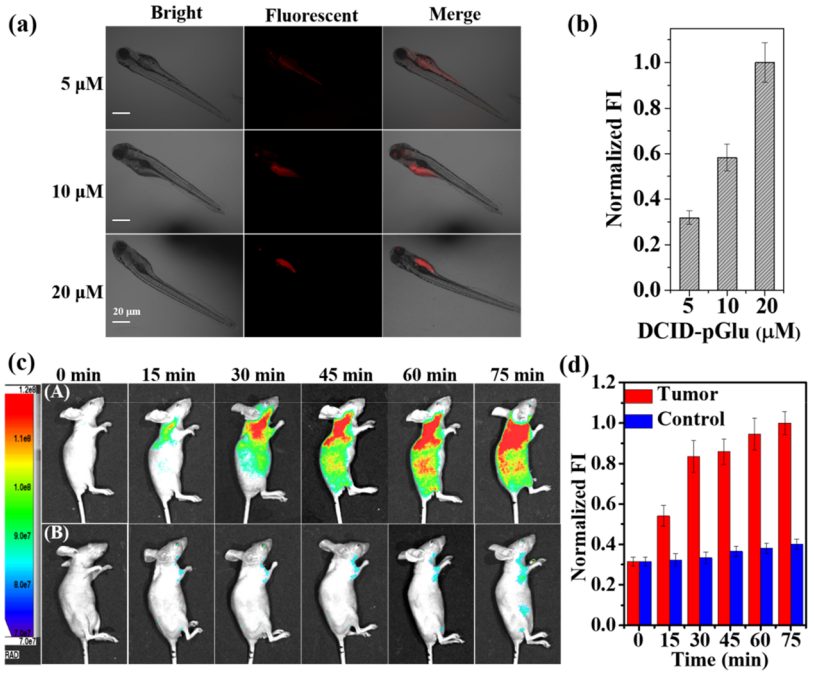

Figure 4. (a) Fluorescence images of PGP-I in living 4-day-old *zebrafish* incubated with different concentrations of **DCID-pGlu** (5, 10, and 20 μM) at room temperature for 4 h. The panels in each group from left to right represent grayscale bright fields, fluorescent fields, and mergeed images of bright fields and fluorescent fields. (b) Relative pixel intensity measurements from images in panel (a) using ImageJ software. (c) *In vivo* real-time fluorescence imaging of endogenous PGP-I in HepG2 tumor-bearing mice (A) and normal nude mice (B) after intravenous injection of **DCID-pGlu** (50, 50 μL). Images were acquired at 0, 15, 30, 45, 60, and 75 min after injection. (d) Relative pixel intensities of images in panel (c) were measured using IDL Virtual Machine software (the pixel intensity at 75 min is defined as 1.0).

cellular PGP-I, we first imaged HuH-7 cells with the developed sensor. The MTT assay revealed that **DCID-pGlu** exhibited good biocompatibility and negligible cytotoxicity to the cells after 24 h coincubation (Figure S13). The incubation of HuH-7 cells with 5 μM **DCID-pGlu** resulted in a robust intracellular fluorescence signal, as monitored by live-cell fluorescence microscopy. The FI increased in a time-dependent manner and reached a plateau within 50 min (Figure 1a,b). Iodoacetamide, a well-known PGP-I inhibitor,[26] was selected to pretreat HuH-7 cells prior to **DCID-pGlu** treatment. As displayed in Figure 1c, the red fluorescence in HuH-7 cells significantly decreased with increasing concentrations of iodoacetamide, suggesting that the fluorescence change indeed resulted from the hydrolysis of **DCID-pGlu** by endogenous PGP-I. Based on the plot of the inhibitory histogram (concentration for half-maximal inhibitory FI), the IC_{50} value was calculated to be ~1.5 μM (Figure 1d). Moreover, other representative small inhibitors of hydrolases, such as bestatin (aminopeptidase N inhibitor) and tacrine (cholinesterase inhibitor), exhibited no substantial perturbation during fluorescence imaging (Figure S14). These results suggest that **DCID-pGlu** could serve as a specific sensor for imaging endogenous PGP-I in living cells with a high resolution and specificity.

3.3. PGP-I Promotes the Proliferation and Migration of HCC Cells by Activating the IL-6/STAT3 Signaling Pathway. Next, the expression levels of PGP-I among various cells, normal cell lines (LO2 and HEK 293), and cancer cell lines (DU145, SKOV3, A549, HCT116, HuH-7, and HepG2) were investigated by **DCID-pGlu** as a sensing tool. As shown in Figure 2, very weak FI was observed in both LO2 and HEK 293 cells, indicating the presence of relatively low levels of endogenous PGP-I in normal cell lines. In contrast, very bright red fluorescence was observed in the four cancer cell lines (HuH-7, HepG2, HCT116, and A549). More interestingly, the two HCC cell lines (HuH-7 and HepG2 cells) showed the strongest fluorescence response, suggesting the elevated intracellular PGP-I expression in liver cancer tumorigenesis. To obtain a clearer illustration, HuH-7 and LO2 cells were combined together and then treated with **DCID-pGlu** simultaneously. As a result, it was easy to distinguish the cell type due to the much stronger red fluorescence in HuH-7 cells than in LO2 cells (Figure S15). Notably, this differentiation was also validated by the bright green fluorescence of green fluorescent protein (GFP)-transfected LO2 cells. These results strongly suggest that PGP-I may be upregulated during HCC progression.

To quantify the dynamic change in cellular PGP-I, two additional cell-based experiments, PGP-I overexpression and knockdown, were also performed to evaluate the sensing capability of **DCID-pGlu**. As shown in Figure 3a,b, HEK 293 cells overexpressing *rh*PGP-I displayed much stronger red fluorescence than that of the control of Lipo (Lipo represents lipofectamine). On the contrary, PGP-I knockdown in HuH-7 cells led to weaker fluorescence emission than that of the control of RNAiMAX (the siRNA transfection agent). Then, we confirmed the overexpression of PGP-I in HEK 293 cells and the reduced expression of PGP-I in siRNA-transfected HuH-7 cells by western blot analysis (Figure 3c). These results demonstrate that **DCID-pGlu** can be regarded as a promising tool to detect and image the dynamic changes in PGP-I expression levels due to biological events.

Tumor cell migration and proliferation are believed to be the two fundamental issues that contribute considerably to the distant metastasis of tumors and tumor microenvironment modulation. To obtain mechanistic insight into the elevated expression of PGP-I in HCC, we probed the migration of

https://doi.org/10.1021/acs.analchem.1c03011
Anal. Chem. 2021, 93, 13311−13318

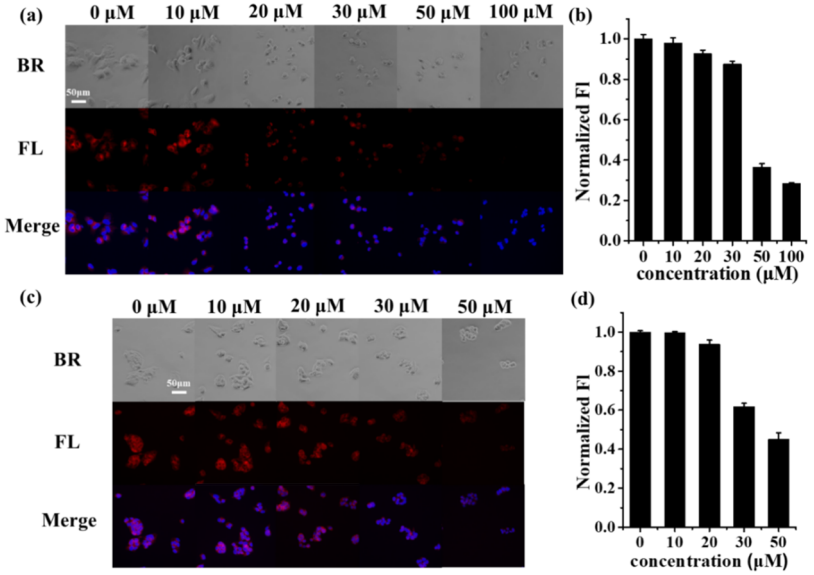

Figure 5. (a) Fluorescence imaging of HuH-7 cells pretreated by gradient concentration of parthenolide (0−100 μM). (b) Relative pixel intensity of the corresponding fluorescence images in panel (a) (the pixel intensity from the image of untreated HuH-7 is normalized as 1.0). (c) Fluorescence imaging of HepG2 cells pretreated with parthenolide of gradient concentration (0−50 μM). (d) Relative pixel intensity of the corresponding fluorescence images in panel (a) (the pixel intensity from the image of untreated HepG2 is normalized as 1.0).

HuH-7 cells with and without PGP-I knockdown. As anticipated, PGP-I knockdown dramatically inhibited the migration and proliferation of HuH-7 cells, which was clearly illustrated by fluorescence imaging with the developed sensor (Figure 3d).

Extensive studies have shown that inflammation plays a key role in HCC progression.[1,7] A better understanding of the molecular processes of inflammation−cancer transformation in HCC development should be quite conducive to HCC diagnosis and drug development. The IL-6/STAT3 pathway plays a key role in the growth and development of various human cancers. Wan et al. demonstrated that IL-6 contributed to the expansion of HCC stem cells via the STAT3 signaling pathway.[27−29] As mentioned earlier, PGP-I was reported to be highly linked to the emergence of inflammation in cells and tissues and was regarded as a new inflammatory cytokine. So, in this study, our major aim is to find the behind molecular mechanism of PGP-I involvement in HCC. Recently, the IL-6/STAT3 signaling axis was reported to be highly associated with HCC.[2,30] STAT3 hyperactivation, especially STAT3 phosphorylation in tumor cells, can occur as a result of elevated IL-6 levels in the serum and/or in the tumor microenvironment, owing to signals from other growth factors. Hence, to understand the association between abnormal levels of PGP-I and the IL-6/STAT3 signaling pathway, we performed western blotting to measure the real PGP-I content in PGP-I-overexpressing HEK 293 cells and PGP-I-knockout HEK 293 cells (Figure 3e,f). When compared to normal HEK 293 cells, the IL-6 expression level was markedly higher in PGP-I-overexpressing cells and was almost undetectable in PGP-I-knockout cells. Meanwhile, the amount of phosphorylated STAT3 was also much higher in PGP-I-overexpressing cells and was strongly alleviated in PGP-I knockout cells, suggesting that elevated PGP-I activated STAT3 phosphorylation and subsequent dimerization. Collectively, these observations imply that PGP-I may promote HCC by targeting the IL-6/STAT3 signaling pathway and could serve as a biomarker for HCC.

3.4. *In Vivo* Real-Time Tracking of PGP-I Activity in *Zebrafish* and Tumor-Bearing Mice. To explore the implication of PGP-I in HCC progression in living organisms, *in vivo* imaging analysis was performed in *zebrafish* and tumor-bearing mice. The *zebrafish* model is a good visual model. In a 4-day-old *zebrafish* model treated with **DCID-pGlu**, bright red fluorescence appeared in *zebrafish*, and the FI increased depending on the concentration of **DCID-pGlu** (Figure 4a,b). To the best of our knowledge, this is the first report that PGP-I exists in *zebrafish* and mainly distributes in the center, which provides a good platform for PGP-I-related bioimaging and the related drug discovery (Table S1). Similarly, in the HepG2 tumor-bearing nude mouse model, the red fluorescence signal was gradually enhanced in a time-dependent manner around the tumor region from 0 to 75 min, whereas the fluorescence signal remained very low in the normal mice (Figure 4c,d). The results demonstrated that **DCID-pGlu** could be developed as a promising tool for *in vivo* real-time PGP-I imaging and the related mechanistic studies.

3.5. Parthenolide-Mediated Inhibition of HCC Cells. Inspired by the above proven correlation between HCC and PGP-I, we hypothesized that PGP-I might be a target for anticancer therapeutics. That is, the antitumor effects of some reported chemical agents for treating HCC may be achieved by the inhibition of PGP-I, particularly inhibitors involved in the IL-6/STAT signaling pathway. Parthenolide, as a natural product, has been reported to be a potent inhibitor of JAK activation with a consequent decrease in the phosphorylated state of STAT3.[31,32] Therefore, parthenolide prevents STAT3 dimerization and accordingly prevents the growth of HCC cells.[33] Our above study showed that PGP-I can activate the phosphorylation of STAT3 and accordingly promote dimerization. To understand the role of parthenolide in the antiproliferation of HCC, HuH-7 cells (Figure 5a,b) and HepG2 (Figure 5c,d) were separately pretreated with various concentrations of parthenolide, followed by imaging with **DCID-pGlu**. Interestingly, the FI significantly decreased with increasing concentrations of parthenolide in two kinds of HCC

https://doi.org/10.1021/acs.analchem.1c03011
Anal. Chem. 2021, 93, 13311−13318

cells (HuH-7 and HepG2 cells). In this regard, we propose that the antitumor effect of parthenolide may be mediated through the inhibition of PGP-I. These observations imply that PGP-I has great potential as a new target for HCC treatment.

4. CONCLUSIONS

In summary, an ultrasensitive biosensor was applied for accurate monitoring and tracing of PGP-I in live cells, *zebrafish*, and HepG2 tumor-bearing mice and was further applied to understand the association of PGP-I with HCC progression. In particular, it was demonstrated that PGP-I promoted HCC by activating the IL-6/STAT3 signaling pathway, which could be alleviated considerably by parthenolide. These results indicated that PGP-I is a potential cancer biomarker and anticancer drug target, and the developed biosensor can serve as an ideal tool for PGP-I-related chemical biology studies and drug discovery. We believe that the PGP-I-activated fluorescence-on probe will be applicable to improving the fundamental understanding of pathogenesis and in the early diagnosis of HCC.

■ ASSOCIATED CONTENT

Supporting Information

The Supporting Information is available free of charge at https://pubs.acs.org/doi/10.1021/acs.analchem.1c03011.

Additional experimental details, materials, and methods; characterization for the chemical structures (Figures S1−S7); kinetics (Figures S8−S13, Table S1); and fluorescence images (Figures S14−S15) (PDF)

■ AUTHOR INFORMATION

Corresponding Author

Wen-Chao Yang − *Key Laboratory of Pesticide & Chemical Biology of Ministry of Education, International Joint Research Center for Intelligent Biosensor Technology and Health, College of Chemistry, Central China Normal University, Wuhan 430079, P. R. China;* orcid.org/0000-0002-6722-0441; Phone: 86-27-67867706; Email: tomyang@mail.ccnu.edu.cn; Fax: 86-27-67867141

Authors

Wu-Yingzheng Guo − *Key Laboratory of Pesticide & Chemical Biology of Ministry of Education, International Joint Research Center for Intelligent Biosensor Technology and Health, College of Chemistry, Central China Normal University, Wuhan 430079, P. R. China*

Rong-Rong Li − *Key Laboratory of Pesticide & Chemical Biology of Ministry of Education, International Joint Research Center for Intelligent Biosensor Technology and Health, College of Chemistry, Central China Normal University, Wuhan 430079, P. R. China*

Yi-Xuan Fu − *Key Laboratory of Pesticide & Chemical Biology of Ministry of Education, International Joint Research Center for Intelligent Biosensor Technology and Health, College of Chemistry, Central China Normal University, Wuhan 430079, P. R. China*

Shi-Yu Liu − *Key Laboratory of Pesticide & Chemical Biology of Ministry of Education, International Joint Research Center for Intelligent Biosensor Technology and Health, College of Chemistry, Central China Normal University, Wuhan 430079, P. R. China*

Guo-Zhen Liu − *Key Laboratory of Pesticide & Chemical Biology of Ministry of Education, International Joint Research Center for Intelligent Biosensor Technology and Health, College of Chemistry, Central China Normal University, Wuhan 430079, P. R. China*

Guang-Fu Yang − *Key Laboratory of Pesticide & Chemical Biology of Ministry of Education, International Joint Research Center for Intelligent Biosensor Technology and Health, College of Chemistry, Central China Normal University, Wuhan 430079, P. R. China;* orcid.org/0000-0003-4384-2593

Complete contact information is available at: https://pubs.acs.org/10.1021/acs.analchem.1c03011

Author Contributions

†W.-Y.G. and R.-R.L. contributed equally to this work.

Notes

The authors declare no competing financial interest.

■ ACKNOWLEDGMENTS

This work was funded by the National Key Research and Development Program of China (No. 2017YFA0505200), the National Natural Science Foundation of China (Nos. 21977036 and U20A2038), and the Hubei Province Natural Science Foundation (No. 2020BHB027).

■ REFERENCES

(1) Llovet, J. M.; Kelley, R. K.; Villanueva, A.; Singal, A. G.; Pikarsky, E.; Roayaie, S.; Lencioni, R.; Koike, K.; Zucman-Rossi, J.; Finn, R. S. *Nat. Rev. Dis. Primers* **2021**, *7*, No. 6.

(2) Dimri, M.; Satyanarayana, A. *Cancers* **2020**, *12*, No. 491.

(3) Berasain, C.; Castillo, J.; Perugorria, M. J.; Latasa, M. U.; Prieto, J.; Avila, M. A. *Ann. N. Y. Acad. Sci.* **2009**, *1155*, 206−221.

(4) Grivennikov, S. I.; Greten, F. R.; Karin, M. *Cell* **2010**, *140*, 883−899.

(5) Ringelhan, M.; Pfister, D.; O'Connor, T.; Pikarsky, E.; Heikenwalder, M. *Nat. Immunol.* **2018**, *19*, 222−232.

(6) Greten, F. R.; Grivennikov, S. I. *Immunity* **2019**, *51*, 27−41.

(7) Chen, H.-J.; Hu, M.-H.; Xu, F.-G.; Xu, H.-J.; She, J.-J.; Xia, H.-P. *Hepatoma Res.* **2018**, *4*, 29.

(8) Doolittle, R. F.; Armentrout, R. W. *Biochemistry* **1968**, *7*, 516−521.

(9) Edman, P.; Högfeldt, E.; Sillén, L. G.; Kinell, P.-O. *Acta Chem. Scand.* **1950**, *4*, 283−293.

(10) Gong, Q.; Li, L.; Wu, X.; Ma, H. *Chem. Sci.* **2016**, *7*, 4694−4697.

(11) Gong, Q.; Zou, R.; Xing, J.; Xiang, L.; Zhang, R.; Wu, A. *Adv. Sci.* **2018**, *5*, No. 1700664.

(12) Cao, T.; Zhang, L.; Ma, H.; Zheng, L.; Cao, Y.; Wang, J.; Yang, Y.; Zhang, J.; Qin, W.; Liu, Y. *Sens. Actuators, B* **2021**, *338*, No. 129841.

(13) De Silva, A. P.; Gunaratne, H. Q. N.; Gunnlaugsson, T.; Huxley, A. J. M.; McCoy, C. P.; Rademacher, J. T.; Rice, T. E. *Chem. Rev.* **1997**, *97*, 1515−1566.

(14) Liu, H. W.; Chen, L.; Xu, C.; Li, Z.; Zhang, H.; Zhang, X. B.; Tan, W. *Chem. Soc. Rev.* **2018**, *47*, 7140−7180.

(15) Singh, H.; Tiwari, K.; Tiwari, R.; Pramanik, S. K.; Das, A. *Chem. Rev.* **2019**, *119*, 11718−11760.

(16) Zhang, J.; Chai, X.; He, X. P.; Kim, H. J.; Yoon, J.; Tian, H. *Chem. Soc. Rev.* **2019**, *48*, 683−722.

(17) Jiao, X.; Li, Y.; Niu, J.; Xie, X.; Wang, X.; Tang, B. *Anal. Chem.* **2018**, *90*, 533−555.

(18) Gao, L.; Wang, W.; Wang, X.; Yang, F.; Xie, L.; Shen, J.; Brimble, M. A.; Xiao, Q.; Yao, S. Q. *Chem. Soc. Rev.* **2021**, *50*, 1219−1250.

(19) Wu, D.; Sedgwick, A. C.; Gunnlaugsson, T.; Akkaya, E. U.; Yoon, J.; James, T. D. *Chem. Soc. Rev.* **2017**, *46*, 7105−7123.
(20) Cao, T.; Zhang, L.; Zheng, L.; Qian, J.; Iqbal, A.; Iqbal, K.; Qin, W.; Liu, Y. *J. Mater. Chem. B* **2021**, *9*, 4546−4554.
(21) Massin, J.; Dayoub, W.; Mulatier, J. C.; Aronica, C.; Bretonnière, Y.; Andraud, C. *Chem. Mater.* **2011**, *23*, 862−873.
(22) Li, H.; Yao, Q.; Sun, W.; Shao, K.; Lu, Y.; Chung, J.; Kim, D.; Fan, J.; Long, S.; Du, J.; Li, Y.; Wang, J.; Yoon, J.; Peng, X. *J. Am. Chem. Soc.* **2020**, *142*, 6381−6389.
(23) Li, H.; Yao, Q.; Pu, Z.; Chung, J.; Ge, H.; Shi, C.; Xu, N.; Xu, F.; Sun, W.; Du, J.; Fan, J.; Wang, J.; Yoon, J.; Peng, X. *Sci. China: Chem.* **2021**, *64*, 499−508.
(24) Liu, T.; Zhang, M.; Feng, L.; Cui, J.; Tian, X.; Yu, Z.; Zhang, B.; Deng, S.; Wang, C.; Ma, X. *B Chem.* **2021**, *337*, No. 129764.
(25) Liu, S. Y.; Xiong, H.; Yang, J. Q.; Yang, S. H.; Li, Y.; Yang, W. C.; Yang, G. F. *ACS Sens.* **2018**, *3*, 2118−2128.
(26) Browne, P.; O'Cuinn, G. *Eur. J. Biochem.* **1983**, *137*, 75−87.
(27) Wan, S.; Zhao, E.; Kryczek, I.; Vatan, L.; Sadovskaya, A.; Ludema, G.; Simeone, D. M.; Zou, W.; Welling, T. H. *Gastroenterology* **2014**, *147*, 1393−1404.
(28) Sun, X.; Sui, Q.; Zhang, C.; Tian, Z.; Zhang, J. *Mol. Cancer Ther.* **2013**, *12*, 2885−2896.
(29) Liu, Y.; Lin, J. *Future Oncol.* **2011**, *7*, 161−164.
(30) Rakoff-Nahoum, S. *Yale J. Biol. Med.* **2006**, *79*, 123−130.
(31) Sun, J.; Zhang, C.; Bao, Y. L.; Wu, Y.; Chen, Z. L.; Yu, C. L.; Huang, Y. X.; Sun, Y.; Zheng, L. H.; Wang, X.; Li, Y. X. *Asian Pac. J. Cancer Prev.* **2014**, *15*, 4897−4902.
(32) Wen, J.; You, K. R.; Lee, S. Y.; Song, C. H.; Kim, D. G. *J. Biol. Chem.* **2002**, *277*, 38954−38964.
(33) Carlisi, D.; D'Anneo, A.; Angileri, L.; Lauricella, M.; Emanuele, S.; Santulli, A.; Vento, R.; Tesoriere, G. *J. Cell. Physiol.* **2011**, *226*, 1632−1641.

https://doi.org/10.1021/acs.analchem.1c03011
Anal. Chem. 2021, 93, 13311−13318